LOW FREQUENCY ASTROPHYSICS FROM SPACE
Proceedings, Crystal City, Virginia 1990

Namir E. Kassim and Kurt W. Weiler (Eds.)

LOW FREQUENCY INTERSTELLAR SCATTERING AND PULSAR OBSERVATIONS

James M. Cordes
Astronomy Department, Cornell University

Radio astronomy at frequencies from 2 to 30 MHz challenges time tested methods for extracting usable information from observations. One fundamental reason for this is that propagation effects due to the magnetoionic ionosphere, interplanetary medium, and interstellar medium (ISM) increase strongly with wavelength. In this paper I address the problems associated with interstellar scattering off of small scale ($\sim 10^9$ cm) irregularities in the electron density.

I will first summarize what we know of interstellar scattering on the basis of high frequency observations, including scintillation and temporal broadening of pulsars and angular broadening of various galactic and extragalactic radio sources. Then I will address those high frequency phenomena that are important or, at least, detectable at low frequencies. The radio sky becomes much simpler at low frequencies: most pulsars will not be seen as time varying sources, intensity variations will be quenched or will occur on time scales much longer than a human lifetime, and many sources will be angularly broadened and/or absorbed into the noise. Angular broadening measurements will help delineate the galactic distribution and power spectrum of small scale electron density irregularities. Images of scattered sources can take on the form of the distribution of the scattering material in this low frequency regime. Spectral broadening may be a relevant line broadening mechanism for low frequency recombination lines.

Summary of Interstellar Scattering and Scintillation Phenomena

Interstellar scattering phenomena are rich in variety. *Diffraction* from small scale irregularities is manifest as angular broadening (interstellar 'seeing'); temporal broadening of pulsar pulses due to multipath propagation; and diffractive intensity scintillations. The latter have been seen only from pulsars owing to their small size (the 'stars twinkle, planets do not' rule: the critical angular size for interstellar scintillation is typically less than 1 *micro* arc sec.) Another effect, as yet unobserved from the ISM, is spectral broadening, the smearing of a spectral line due to modulations imposed by the diffracting medium. *Refraction* effects from larger irregularities include long term scintillations; wandering of apparent source positions on the sky (angle of arrival [AOA] variations); and time of arrival variations associated with the AOA variations and also with the changing electron column density (the dispersion measure, DM) as turbulence is swept across the line of sight. Figure 1 shows examples of several of these phenomena, including the visibility function of a scattered pulsar; temporal broadening of a pulsar pulse; diffractive intensity scintillations; and dispersion measure variations.

There is substantial evidence that the electron density variations responsible for the phenomena span a large range of length scale and that they may be described by a

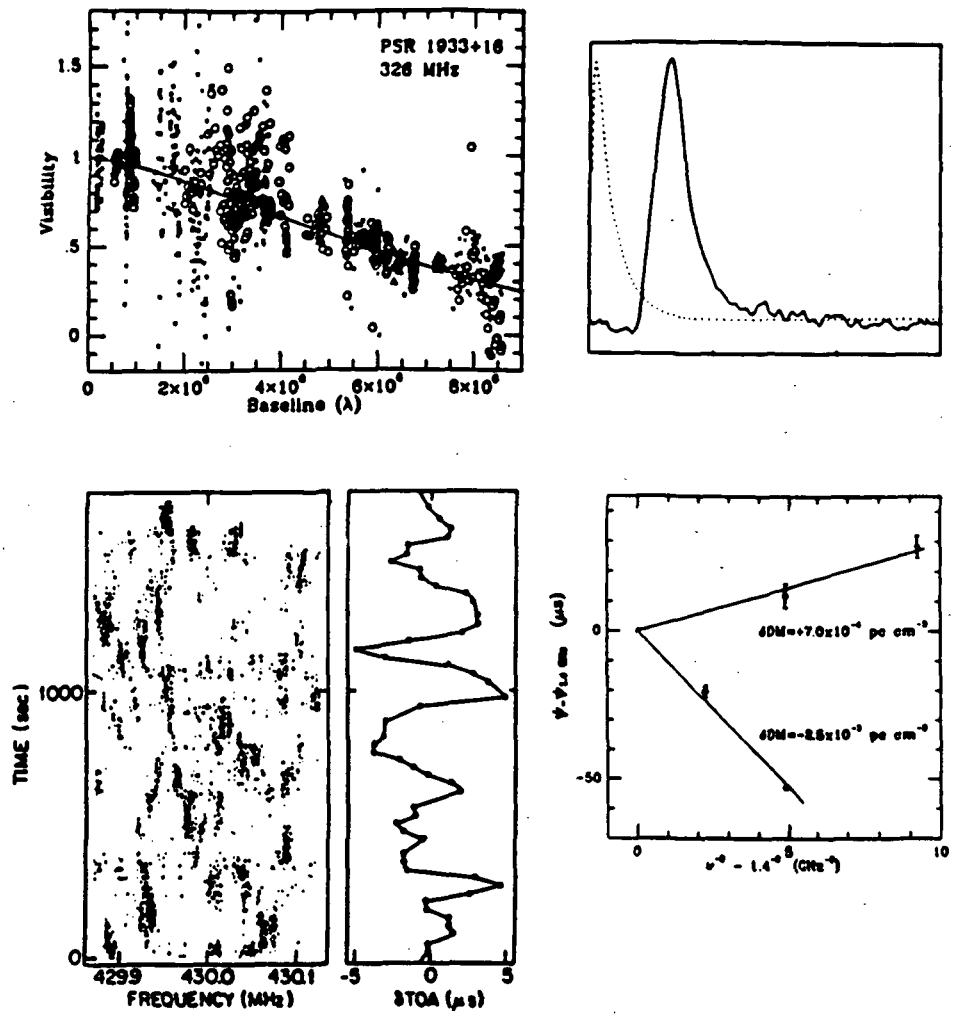

Figure 1. Examples of scattering observables: (a) visibility function[1]; (b) pulsar pulse with scattering broadening tail[2]; (c) grey scale plot of diffractive intensity scintillations[3]; (d) dispersion measure variations[4].

spatial power spectrum that is power law in form. Thus we define the power spectrum in terms of the mean square electron density:

$$\langle \delta n_e^2 \rangle \equiv \int_{q_0}^{q_1} d^3q \, C_n^2 \, q^{-\alpha}, \tag{1}$$

where we introduce the coefficient C_n^2, wavenumber cutoffs $q_{1,2}$, and spectral index α. Pulsar scintillations and time of arrival variations, and limits on AOA variations of OH masers[5] imply that $3.5 \leq \alpha \leq 4.0$. The Kolmogorov value, $\alpha = 11/3$, is consistent with many lines of sight. Defining, respectively, the 'inner' and 'outer' length scales $\ell_1 = 2\pi/q_1$ and $\ell_0 = 2\pi/q_0$ of the spectrum, limits from several kinds of observations suggest that $\ell_1 \leq 10^9$ cm and $\ell_0 \geq 10^{14}$ cm. Recent work[5,6,7] suggests that the inner scale is of the order of 100 km for a few heavily scattered lines of sight, a length scale consistent with the gyro radius of thermal ions in the warm (10^4 K) phase of the ISM. There are indirect arguments that the outer scale extends to parsec scales, based on studies of rotation measure variations[8] and on the notion that cosmic ray diffusion

requires magnetic irregularities on all scales from about 1 AU to 1 pc and that these are accompanied by density irregularities[9].

The easiest quantity to estimate, given the spectral index α, which we now assume to be 11/3, is the line of sight integral of C_n^2, which we call the *scattering measure*. The scattering measure and estimates of it using angular scattering diameters of extragalactic sources θ_{FWHM} and pulsar temporal broadening times τ_d are:

$$SM \equiv \int_0^D ds\, C_n^2(s) = \left(\frac{\theta_{FWHM}}{\theta_0}\right)^{5/3} \nu^{11/3} = A_\tau \left(\frac{\tau_d}{D}\right)^{5/6} \nu^{11/3},$$

where $\theta_0 = 0.13$ arc sec, $A_\tau = 387$ kpc $\mathrm{m}^{-20/3}$ for τ_d in seconds and D in kpc, and ν in GHz. Measured values of SM range from 10^{-4} to 10^3 kpc $\mathrm{m}^{-20/3}$. For scintillation bandwidth measurements, SM may be estimated by first using the 'uncertainty' relationship $2\pi\Delta\nu_d\tau_d = 1$ to estimate the effective temporal broadening time. For a pulsar embedded in a homogenously turbulent medium, we have

$$\theta_{FWHM} = \left[\frac{16(\ell n 2)c\tau_d}{\pi D}\right]^{1/2}.$$

In terms of the scattering diameter, the diffraction scale is $\ell_d = 2\sqrt{\ell n 2}\lambda/\pi\theta_{FWHM}$.

Spectral broadening is approximately equal to the reciprocal of the intensity scintillation time; both are due to modulations of the signal due to motion of diffracting material across the line of sight. In terms of SM, the broadening is[10]

$$\Delta\nu_s \approx \frac{V_\perp}{\ell_d} \approx 2\pi V_\perp [4\pi r_e^2 \lambda^2 C_n^2 D]^{3/5} = 1.16 \text{ Hz } V_{100}\nu^{-6/5} SM^{3/5},$$

where r_e is the classical electron radius, $V_\perp$ is the relevant transverse speed (a combination of pulsar, ISM, and Earth velocities), V_{100} is in units of 100 km s^{-1}, and SM has units of *kpc* $m^{-20/3}$, and ν is in GHz.

For galactic objects with known distances, we obtain the line of sight average $\overline{C_n^2} \equiv SM/D$. The remarkable fact is that $\overline{C_n^2}$ varies by a factor of at least 10^4 between different lines of sight. A homogenously turbulent medium would, of course, yield a constant value for this quantity. Figure 2 shows SM plotted against galactic latitude and longitude on an equal area projection. The plotted circles have diameters that are proportional to $\log SM$. It is obvious that scattering is a galactic phenomenon, since the largest circles are on lines of sight in the galactic plane. Study of how SM varies (work in progress) implies that the variation in $\overline{C_n^2}$ is due to both large scale galactic structure and localized regions of intense turbulence, including HII regions and supernova remnants. Enhanced scattering seems to be correlated over small angular scales, implying that the depth is of order a few parsecs or less. This implies that the internal C_n^2 of enhanced regions is correspondingly larger than $\overline{C_n^2}$ by a factor of about 1000.

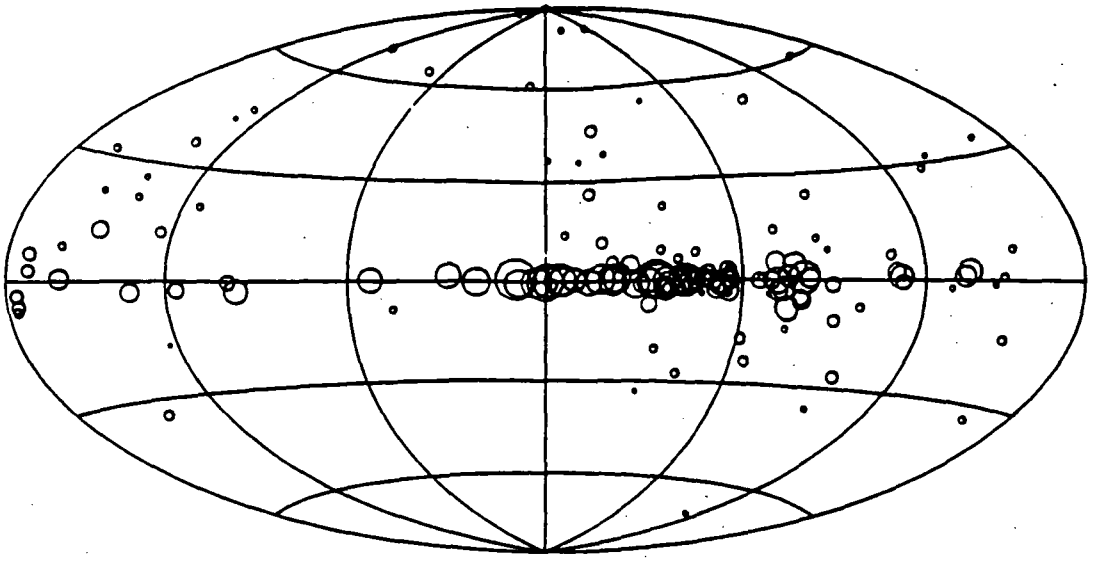

Figure 2. Scattering measures plotted versus ℓ, b; $\log SM = 3$ for the largest circles, the smallest circles have $\log SM = -4$.

To make estimates of low frequency scattering phenomena, it is useful to fit an idealized model to the data. The *local* value of C_n^2 at galactocentric radius R and distance z from the galactic plane comprises two components:

$$C_n^2(R,z) = C_1 \exp[-(R^2/A_1^2 + z/H_1)] + C_2 \exp[-(R^2/A_2^2 + z/H_2)].$$

A grid search to minimize the mean square difference between predicted and measured SM yields a large scale component with $A_1 \gtrsim 10$ kpc and $H_1 \approx 1$ kpc and a galactic center component with $A_2 \approx 3.0$ kpc and $H_2 \approx 0.05$ kpc. The strengths of the two components are $C_1 \approx 10^{-4}$ m$^{-20/3}$ and $C_2 \approx 5$ m$^{-20/3}$. This model accounts for the broad brush structure that determines SM, but there are substantial departures from the model's predictions. Figure 3 shows the modeled SM plotted against measured SM. Notable lines of sight that deviate from the model by more than two orders of magnitude include the Vela pulsar[11]; Cygnus X-3 (ref 6); and the extragalactic source behind the HII complex NGC6334B (ref 5). The grid search was iterated several times so that 'deviant' sources could be recognized and excluded from the fit. The numbers quoted above derive from the end result of this process. In a later section, the model is used to predict observable quantities such as angular broadening, spectral broadening, and temporal broadening.

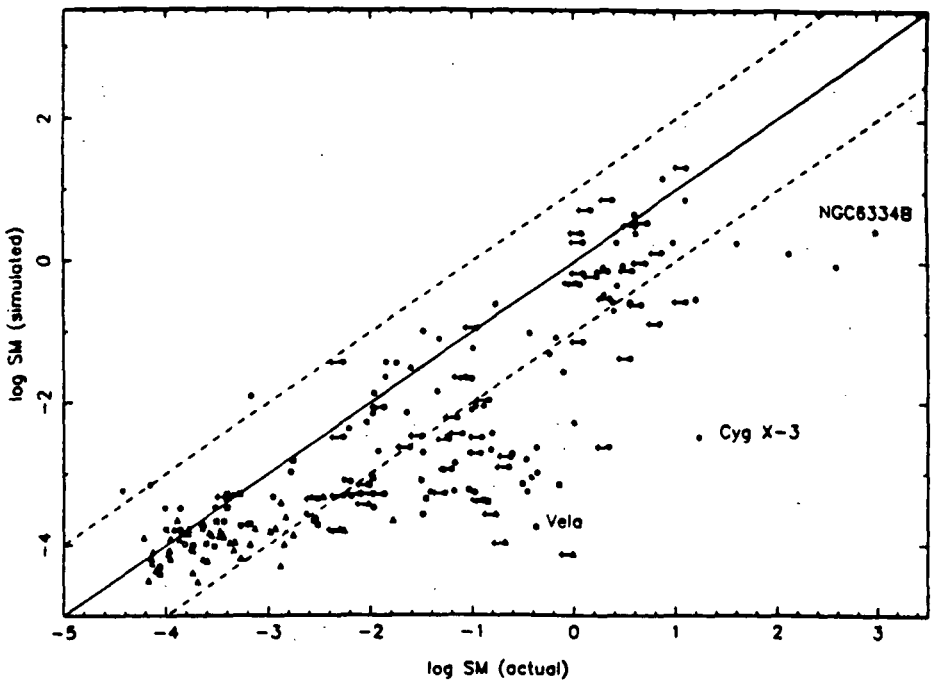

Figure 3. Modeled SM plotted against actual SM. A few notable lines of sight are labeled.

TABLE 1
DIFFRACTION PHENOMENA

Phenomenon	Quantity	Typical Values		
		400 MHz	30 MHz	10 MHz
Intensity Scintillations	$\Delta\nu \propto \lambda^{-4.4}$	10 kHz	10^{-2}	10^{-7}
	$\Delta t_d \propto \lambda^{-1.2}$	60 sec	3	0.7
Temporal broadening	$\tau_d \propto \lambda^{4.4}$	1 ms	1 min	3 hr
Angular broadening	$\theta_d \propto \lambda^{2.2}$	10 $m.a.s.$	3″	33″
Spectral broadening	$\Delta\nu_s \propto \lambda^{1.2}$	1 Hz	22	83

TABLE 2
REFRACTION PHENOMENA

Phenomenon	Quantity	Typical Values		
		400 MHz	30 MHz	10 MHz
Slow scintillations	$\sigma_I/I \propto \lambda^{-1.1}$	20%	1	0.3
	$\Delta t_r \propto \lambda^{2.2}$	1 yr	300	3000
Time-of-arrival variations	$\Delta t_{DM} \propto \lambda^2$	10μs	2 ms	16 ms
	$\Delta t_\theta \propto \lambda^{1.6}$	1μs	60	400
	$\Delta t_{\theta^2} \propto \lambda^{3.3}$	1μs	5 ms	200 ms
Angular wandering	$\Delta\theta_r \propto \lambda^{1.6}$	1 $m.a.s.$	60	400

Interstellar Scattering at Low Frequencies

Using results from high frequency observations and our understanding of the scattering medium's spectrum and distribution, it is possible to discuss the phenomena at low frequencies. In Table 1 the scaling laws[12] for various diffraction phenomena are presented and representative values of the observables are given. Intensity scintillations, which have typical frequency and time scales of 10 kHz and 60 sec at meter wavelengths become sub-Hz and subsecond at 10 MHz. In order to detect intensity scintillations, a radiometer must have sufficient signal to noise ratio for the frequency and time resolution necessary to resolve the scintillations in both time and frequency. At low frequencies where system temperatures are determined by the sky background, it is clear that diffractive scintillations will never be detectable, even for the nearest pulsar, which has the largest scintillation bandwidth. Temporal broadening becomes much larger than the pulse period of almost all pulsars at 10 MHz, so pulsars will be seen as steady sources. Angular broadening becomes a few to many arc seconds. Spectral broadening may be important for recombination line observations.

Figure 4 details the observed scattering broadening times of pulsars, showing τ_d plotted against DM . Data are taken from the literature and have been scaled to 1 GHz assuming the Kolmogorov scaling $\tau_d \propto \lambda^{22/5}$. To assess the level of temporal broadening at low frequencies, horizontal lines have been drawn (again using the Kolmogorov scaling) to show 1 sec of broadening at 10 and 30 MHz. The meaning of these lines is that all pulsars above each horizontal line will be essentially smeared out, since the average pulsar period is ~ 0.7 sec. At 10 MHz, there are only 2 pulsars below the line, while at

30 MHz, a few tens of objects are below the line. At 2 MHz, all pulsars are well above the 1 sec line (not shown). It is amusing to consider the most broadened pulsar (PSR 1849+00; ref 13) which has 1 sec of broadening even at 1 GHz. The formal scaling to 1 MHz, yields a broadening of 0.5 Myr! Note, however, that the scaling law $\tau_d \propto \lambda^{22/5}$ is based on a small angle approximation[14], which breaks down for heavily scattered lines of sight at low frequencies. Relaxing the small angle approximation gives a more reasonable result: only about 20 kyr! This means that the distribution of paths along which radiation propagates subtends a major fraction of the galactic disk. Of course, this is an academic exercise, since no source will be observable along such heavily scattered lines of sight due to free free absorption (see below).

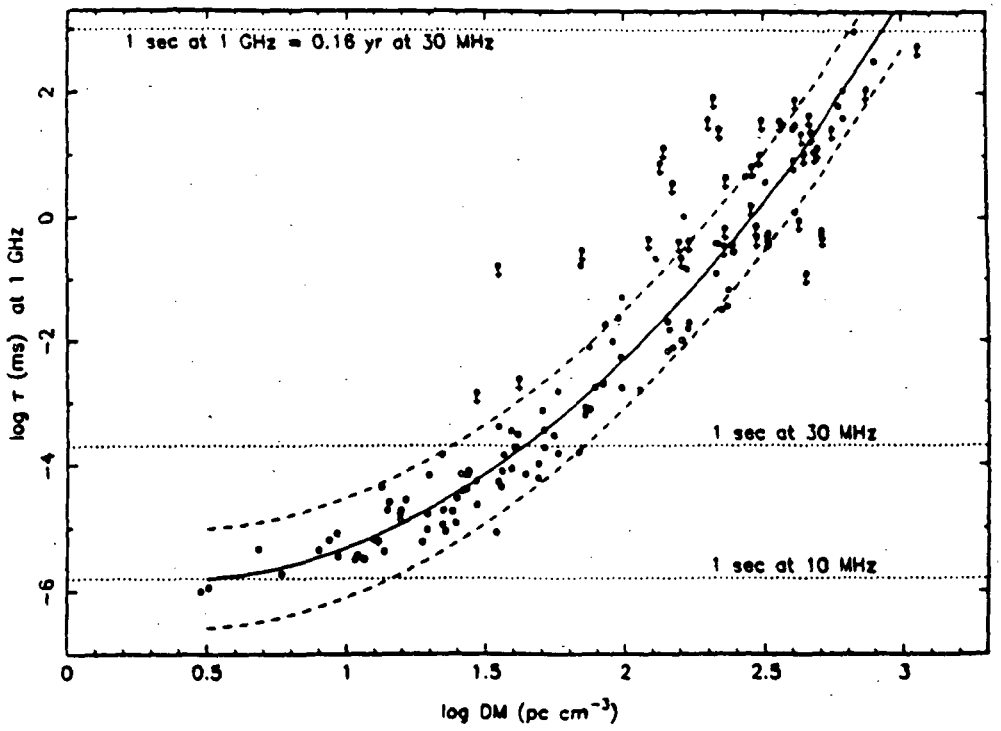

Figure 4. Pulsar temporal broadening times plotted against dispersion measure, DM. The solid line is a least squares fit to the data; the dashed lines are $\pm 1\sigma$ deviations from the fit. Downward arrows denote upper limits, which were excluded from the fit.

Refraction phenomena are presented in Table 2. Refractive scintillations occur on time scales measured in hundreds of years, so even the most dedicated of monitorers will be thwarted in variability studies. Angle of arrival variations and the associated time of arrival variations scale more slowly with wavelength than do angular and temporal broadening. As a consequence, these variations will be proportionally smaller than the angular size or pulse width and thus extremely difficult to measure at low frequencies.

Predicted Observables at Low Frequencies

The net implications for low frequency radio astronomy are that: (1) Diffractive intensity scintillations will be quenched for realistic instrumental bandwidths and time constants. This means that the equivalent of speckle interferometry in the radio will

not be possible in imaging observations. (2) Pulsar periodicities will be quenched by temporal broadening. This statement holds for all pulsars at 2 MHz, all but a few at 10 MHz, and for most at 30 MHz. (3) The time scale of refractive phenomena is much longer than a scientific career. The radio sky indeed will appear quiesent compared to high frequencies. (4) The dominant observable will therefore be the angular broadening of all kinds of radio sources. For a few pulsars in the 10 to 30 MHz band, temporal broadening can be measured, leading to determinations of the scaling law of the temporal broadening, in turn leading to further constraints on the slope and cutoffs of the wavenumber spectrum. Also, for a few pulsars, it will be possible to test whether time of arrival variations that depend on wavelength follow the λ^2 dependence of the cold plasma dispersion law, or whether TOA variations due to AOA variations are also important. These last tests will help constrain the wavenumber spectrum for δn_e on scales much larger than 1 AU. (5) Sources viewed at low galactic latitudes will be so scattered that their shapes will take on the form of the distribution of scattering material, viz. the galactic plane. This is because the maximum traversal of a ray transverse to the propagation direction is limited by the extent of the scattering medium. This source of image asymmetry has not been addressed before and competes with asymmetries due to anisotropies of the small scale irregularities themselves and distortion of a scattered image by refraction[15,16].

Using the idealized model for $C_n^2(R,z)$ discussed above, it is possible to predict the values of the most important observables at low frequencies, namely the angular broadening diameter θ_{FWHM} and the spectral broadening $\Delta\nu_c$. Figure 5 shows the angular broadening plotted against galactic latitude for several cuts in longitude.

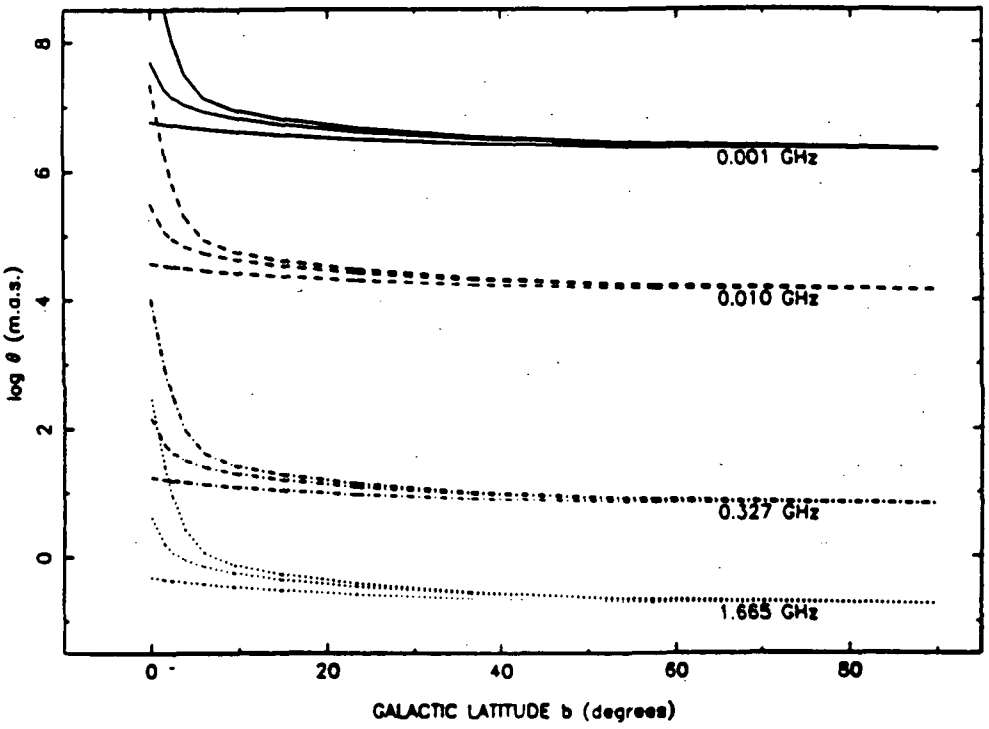

Figure 5. Predicted angular broadening of extragalactic sources vs. galactic latitude for different frequencies and for three longitudes (0, 60, and 180°.)

Spectral broadening takes on values of 300, 20, and 5 kHz at observing frequencies of 1, 10, and 30 MHz for the largest observed scattering measure (10^3 *kpc* $m^{-20/3}$ for NGC6334B, ref 5). This broadening corresponds to velocity spreads of 10^5, 500, and 50 km s^{-1}. At high latitudes, the spectral broadening is a factor of 10^4 smaller and is therefore negligible.

The spectrum defined in equation (1) implies a *lower bound* on the emission measure for a given line of sight. The total emission measure is:

$$EM = \int_0^D ds\,\langle n_e^2\rangle = \int_0^D ds\,\left[\langle n_e\rangle^2 + \langle(\delta n_e)^2\rangle\right] \equiv EM_0 + EM_\delta .$$

The line of sight integral of equation (1) gives the second term on the right hand side of the above equation. The integral of eqn (1) is

$$\langle(\delta n_e)^2\rangle = \frac{4\pi(2\pi)^{3-\alpha}}{\alpha-3} C_n^2 \ell_0^{\alpha-3}\left[1-\left(\frac{\ell_1}{\ell_0}\right)^{\alpha-3}\right] \approx \frac{4\pi}{\alpha-3} C_n^2 \left(\frac{\ell_0}{2\pi}\right)^{\alpha-1} .$$

for $\alpha \neq 3$, where the approximate equality holds for the inner scale being much smaller than the outer scale, $\ell_1 \ll \ell_0$, which seems to be a good approximation. For $\alpha = 11/3$ we have

$$EM_\delta \approx 544\,\mathrm{pc\ cm^{-6}}\ SM(\mathrm{kpc\ m^{-20/3}})\,[\ell_0(\mathrm{pc})]^{2/3} .$$

The measured values of SM therefore imply minimum emission measures of 0.05 to 10^5 pc cm^{-6} if we assume an outer scale of 1 pc. In Figure 6 we show EM_δ plotted against ℓ, b using an outer scale of 100 pc as would be measured along the lines of sight to extragalactic sources. Lines are also drawn that designate optical depth unity for several radio frequencies. It is clear that much of the Galaxy is opaque at these low frequencies. It is of interest to compare the predicted minimum EM with measured values of Reynolds[17]. For $|b| = 90°$, Reynolds obtains $EM \approx 4$ pc cm^{-6} while the scattering measurements suggest $EM_\delta(|b| = 90°) \approx 0.11\ell_0^{2/3}$. If we assume that $EM_0 \approx EM_\delta$, then an outer scale of $\ell_0 \approx 100$ pc is implied. Such an outer scale is consistent with other conjectures about the overall extent in wavenumber of the electron density spectrum[18,19].

References

1. Gwinn, C.R., Cordes, J.M., Bartel, N., and Wolszczan, A. 1988, *Ap. J. (Letters)*, **334**, L13.

2. Cordes, J.M., Weisberg, and Boriakoff, V. 1985; *Ap. J.*, **288**, 221.

3. Cordes, J.M., Wolszczan, A., Dewey, R. J., Blaskiewicz, M., and Stinebring, D. R. 1990; *Ap. J.*, **349**, 245. See also Rawley, L.A., Taylor, J. H., and Davis, M.M. 1988, *Ap. J.*, **326**, 947.

4. Gwinn, C.R., Moran, J. M., Reid, M. J., Schneps, M. H. 1988, *Ap. J.*, **330**, 817.

5. Moran, J.M., Rodriquez, L. F., Greene, B. and Backer, D.C. 1989, *Ap. J.*, in press.

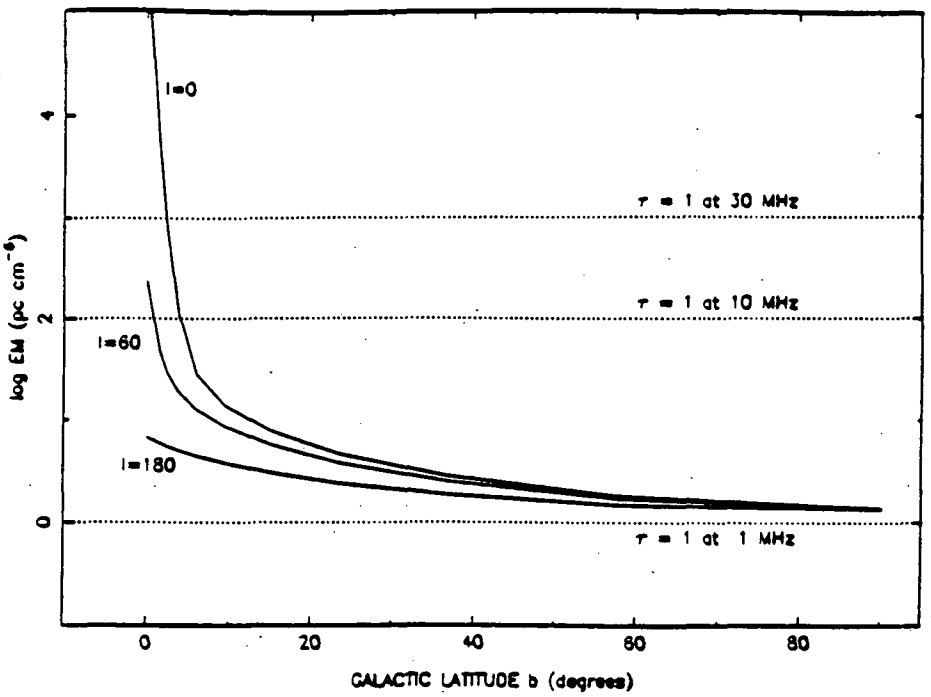

Figure 6. Predicted minimum emission measure vs. galactic coordinates.

6. Molnar, L. A., Mutel, R. L., Reid, M. J., and Johnston, K. J. 1990, *Ap. J.*, submitted.

7. Spangler, S.R. and Gwinn, C.R. 1990, *Ap. J.*, in press.

8. Simonetti, J. H., Cordes, J.M., and Spangler, S.R. 1984, *Ap. J.*, **284**, 126; Lazio, J., Spangler, S.R., and Cordes, J.M., *Ap.J.*, in press.

9. Jokipii, J. R. 1988, in AIP Proceedings 174, *Radio Wave Scattering in the Interstellar Medium*, 48.

10. Lazio, J. and Cordes, J.M., in preparation.

11. Backer, D. C. 1974; *Ap. J.*, **190**, 667.

12. Cordes, J. M., Pidwerbetsky, A., and Lovelace, R.V. 1986, *Ap. J.*, **310**, 737. See also Romani, R., Narayan, R., and Blandford, R. D. 1986, *M.N.R.A.S.*, **220**, 19; Foster, R. S. and Cordes, J. M. 1990, *Ap. J.*, submitted.

13. Clifton, T. 1985, Ph.D. Thesis, Univ. of Manchester.

14. Rickett, B. J. 1977, *Ann. Rev. Ast. Ap.*, **15**, 479.

15. Spangler, S. R. and Cordes, J. M. 1988, *Ap. J.*, **332**, 346.

16. Narayan, R. and Goodman, J. 1989, *M.N.R.A.S.*, **238**, 963.

17. Reynolds, R. J. 1990, these proceedings.

18. Armstrong, J. W., Cordes, J. M., and Rickett, B. J. 1981, *Nature*, **291**, 561.

19. Lee, L.C. and Jokipii, J. R. 1976, *Ap. J.*, **206**, 735.